Multi-wavelength study of MGRO J2019+37 *

HOU Chao(侯超)[1)] CHEN Song-Zhan(陈松战) YUAN Qiang(袁强) CAO Zhen(曹臻)
HE Hui-Hai(何会海) SHENG Xiang-Dong(盛祥东)

Institute of High Energy Physics, Chinese Academy of Sciences, Beijing 100049, China

Abstract: MGRO J2019+37, within the Cygnus region, is a bright extended source revealed by Milagro at 12–35 TeV. This source is almost as bright as the Crab Nebula in the northern sky, but is not confirmed by ARGO-YBJ around the TeV scale. Up to now, no obvious counterpart at low energy wavelengths has been found. Hence, MGRO J2019+37 is a rather mysterious object and its VHE γ-ray emission mechanism is worth investigating. In this paper, a brief summary of the multi-wavelength observations from radio to γ-rays is presented. All the available data from XMM-Newton and INTEGRAL at X-ray, and Fermi-LAT at γ-ray bands, are used to get constraints on its emission flux at low energy wavelengths. Then, its possible counterparts and the VHE emission mechanism are discussed.

Key words: MGRO J2019+37, multi-wavelength, VHE γ-ray, radiation mechanism

PACS: 98.70.Rz, 95.55.Ka, 95.30.Gv **DOI:** 10.1088/1674-1137/38/8/085001

1 Introduction

The Cygnus region is an active massive star formation and destruction portion on the Galactic plane, with coordinate range of ($l \in [65°,85°]$, $b \in [-2°,+2°]$) and distance of 1–2 kpc from us. It is the brightest diffuse γ-ray source in the northern sky as revealed by Fermi-LAT at GeV, ARGO-YBJ at TeV and Milagro at 15 TeV [1–3]. As it contains a large number of molecular clouds and is rich in potential cosmic-ray acceleration sites, such as Wolf-Rayet stars, OB associations andsupernova remnants, the Cygnus region is of great interest for scientists studying the origin of cosmic rays [4, 5].

MGRO J2019+37, detected by Milagro within the Cygnus region, is towards the Cyg OB1 association. It is the brightest of the three new extended sources discovered by the Milagro experiment when it surveyed the northern Galactic plane [6]. Its extension is $\sigma = 0.32°\pm0.12°$ for a symmetric two-dimensional Gaussian shape. Its measured flux is about 80% Crab unit at 20 TeV [7]. This source is suspected to be associated with the GeV pulsar J2021+3651 [8]. About 0.9° away from MGRO J2019+37, the Tibet ASγ collaboration reported a preliminary 5.8σ excess in [9], while only a marginal signal was reported in their later formal result [10, 11].

The ARGO-YBJ experiment is a full coverage extensive air shower (EAS) array with a large field of view (FOV) at a high altitude of 4300 m. The threshold is around 300 GeV, which is much lower than any previous EAS arrays. The other two bright extended sources discovered by Milagro, i.e., MGRO J2031+41 and MGRO J1908+06, have been confirmed by ARGO-YBJ with significance greater than 5σ [5, 12, 13]. MGRO J2031+41 is also located in the Cygnus region near MGRO J2019+37. The energy spectra of these two sources measured by ARGO-YBJ are consistent with those measured by Milagro. Besides these, ARGO-YBJ detected another extended source HESS J1841−055 [14]. Unexpectedly, ARGO-YBJ detected little signal from the brightest Milagro source MGRO J2019+37, and the derived flux upper limits at the 90% confidence level (c.l.) are lower than the Milagro flux at energies below 5 TeV [5]. The ARGO-YBJ upper limits do not conflict with the Milagro 1σ error region in a new analysis applied to the Milagro data from 2005 to 2008 [15], while they constrain that the flux should be lower than the best-fitting value derived by Milagro. In such a situation, a peak structure is formed with the energy as high as about 10 TeV.

VERITAS is a narrow FOV imaging atmospheric Cherenkov telescope with excellent energy and angular resolution ranging from hundreds of GeV to multi TeV. In 2007, VERITAS had surveyed the Cygnus region with a sensitivity of 6.3% Crab unit, but no emission from MGRO J2019+37 was detected [16]. In 2010, with further deep observations better than 1% Crab unit,

Received 11 March 2014

∗ Supported by National Natural Science Foundation of China (11205165, 11375210) and Xiejialin Fund of Institute of High Energy Physics, Chinese Academy of Sciences (Y3546140U2)

1) E-mail: houchao@ihep.ac.cn

VERITAS revealed a complex TeV emitting structure at the position of MGRO J2019+37, which is likely powered by multiple sources [17].

The MGRO J2019+37 region was surveyed by the Giant Metrewave Radio Telescope (GMRT) at the frequency of 610 MHz and the 3.5 m telescope in Calar Alto at the near-infrared K_s-band. A catalogue of 362 radio sources and $\sim 3\times10^5$ near-infrared sources were detected [18]. Some peculiar sources are noticeable, such as the pulsar PSR J2021+3651, two new radio-jet sources, the radio source NVSS J202032+363158 and the HII region Sh 2-104 containing two star clusters.

The MGRO J2019+37 region was also observed with high sensitivity by XMM-Newton at 1–8 keV. A $\sim$20' extended emission around PSR J2021+3651 and an UCHII region in Sh 2-104 were detected. In the GeV band, EGRET, Fermi-LAT and AGILE all detected some point sources with this extended region. Among them, PSR J2021+3651 detected by Fermi-LAT is a spin-powered radio pulsar whose spectrum has a cutoff at 10 GeV.

To sum up, no similar morphology as that of the TeV emission is found at radio, optical, X-ray and GeV γ-ray bands. Therefore, no definite counterpart of MGRO J2019+37 is found at low energy bands.

The existing observations by low energy band telescopes do not give a flux constraint, especially for the MGRO J2019+37 extended region. In order to better understand the TeV emission mechanism, a multi-wavelength observation, especially at X-ray and γ-ray bands, is necessary. For such a large extended region, observations for MGRO J2019+37 should be implemented by detectors with wide FOV. In this paper, all the available data from INTEGRAL at hard X-ray and Fermi-LAT at γ-ray bands, which are wide FOV, are used to constrain the emission flux from MGRO J2019+37. In addition, the soft X-ray data from the narrow FOV detector XMM-Newton are also analyzed. Its possible origins and the corresponding emission mechanism are then discussed.

2 Multi-wavelength analysis

Since the angular resolution of ground-based particle detectors is relatively poor, it is difficult to identify the low energy counterpart of a TeV γ-ray source given there is usually more than one low energy source in the error box of the TeV source. Variability is a good identifier to find the counterpart for variable sources. However, it becomes more difficult for a steady source. In this case, we may need a more detailed study of the properties of all the observed sources, such as spectrum, flux, pulsation and even polarization to explore their possible connection with the target source. In the following, we try to find the low energy counterpart of MGRO J2019+37 and discuss its multi-wavelength emission mechanism.

2.1 Fermi-LAT GeV gamma-ray

Fermi-LAT is a high-energy γ-ray telescope covering the energy band from 20 MeV to 300 GeV. The angular resolution is about 3.5° at 100 MeV, improved to about 0.1° at 10 GeV [19]. The FOV of Fermi-LAT covers about 20% of the sky at a time. It scans continuously, and covers the whole sky every three hours. The LAT data from a region of interest (ROI) centered on MGRO J2019+37 (304.63°,36.88°) with a radius of 20° were downloaded from Fermi Science Support Center[1)]. The observation time is from 4 August 2008 to 4 August 2012.

The data analysis was performed following the standard procedure with a binned maximum-likelihood method. The model adopted in the likelihood fitting included the diffuse backgrounds with both the Galactic and isotropic components, as well as the point sources in the 2FGL catalog [1]. Within a 1° region of MGRO J2019+37, there are three point sources in the 2FGL catalog, which are 2FGL J2021+3651, 2FGL J2018+3626 and 2FGL J2015.6+3709. 2FGL J2021+3651 is identified as a pulsar, and 2FGL J2015.6+3709 is identified as an active galactic nucleus (AGN). 2FGL J2018+3626 is unidentified, and it may be the counterpart of MGRO J2019+37.

The left panel of Fig. 1 shows the residual γ-ray counts map of the sky around MGRO J2019+37, after subtracting the diffuse backgrounds. To reduce the influence of pulsar PSR J2021+3651, which has a spectral cutoff at about 10 GeV [20], we adopt an energy threshold of 10 GeV to show the counts map and for the spectral analysis below. The counts map is smoothed with a 0.3° width Gaussian kernel. From the counts map we see that 2FGL J2018+3626 has few photons above 10 GeV. The spectrum given in the 2FGL catalog for this source is also very soft at high energies. Since the other two sources located in the vicinity of MGRO J2019+37 have been identified as a pulsar and an AGN, we think that none of these three sources will serve as the counterpart of MGRO J2019+37. The right panel of Fig. 1 gives the residual map after further subtracting the known 2FGL sources. It shows that there is not any excess at the location of MGRO J2019+37.

We then add MGRO J2019+37 to the model and redo the likelihood analysis. MGRO J2019+37 is modeled with a two-dimensional Gaussian template with σ=0.35° as revealed in the TeV observation [6]. No strong signal with significance $>2\sigma$ is found. We therefore derive the upper limits of MGRO J2019+37 with Fermi-LAT data. Assuming a power-law index of 2, we find the 95% c.l.

1) http://fermi.gsfc.nasa.gov/ssc/

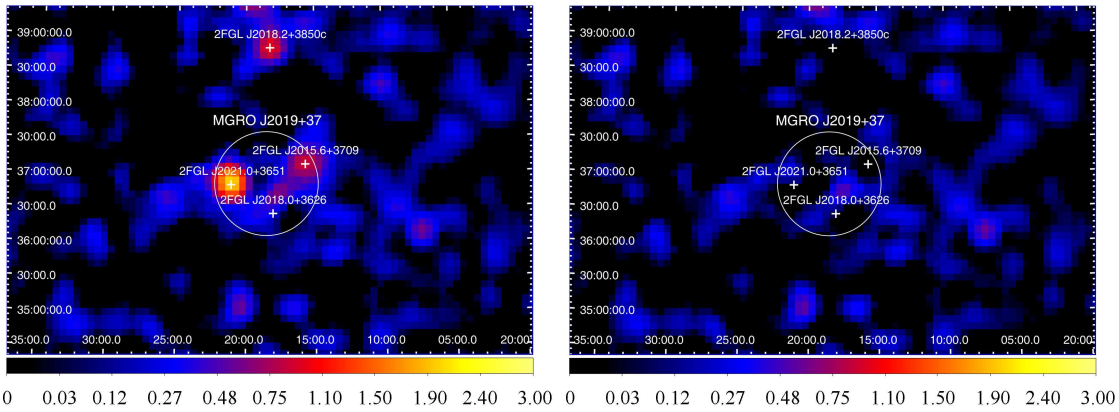

Fig. 1. (color online) Residual counts map (in square root scale) of γ-ray photons above 10 GeV using the data observed by Fermi-LAT, after subtracting the diffuse backgrounds (left) and the diffuse backgrounds together with the known 2FGL sources (right). The circle shows the target region of MGRO J2019+37 with diameter of 1°, and the crosses label the known sources in the LAT 2FGL catalog.

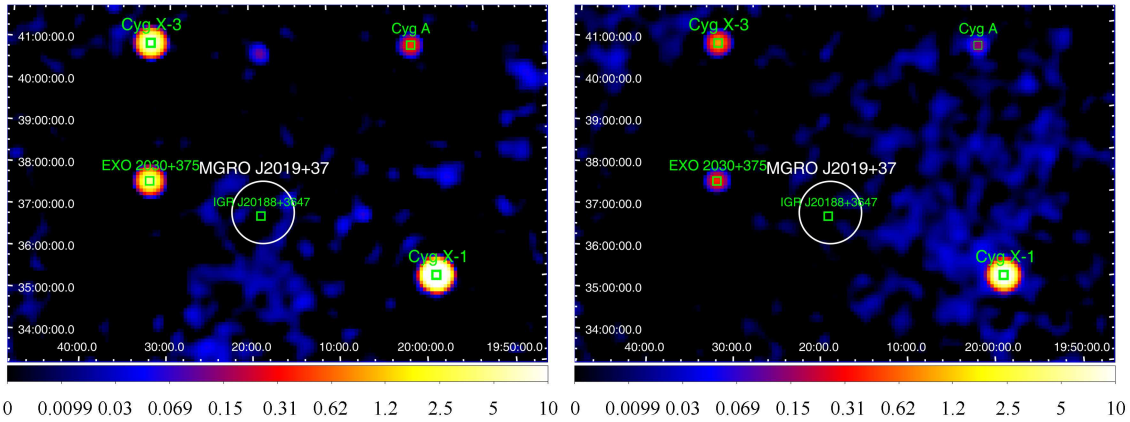

Fig. 2. (color online) Count rate map (in logarithmic scale) of X-ray photons using the data observed by INTEGRAL IBIS/ISGRI from 2002 to 2012, smoothed with a 0.25° Gaussian kernel. The left panel is for 20−60 keV, and the right panel is for 60−200 keV. The circle shows the target region of MGRO J2019+37 with diameter of 1°, and the squares represent the positions of known sources in the INTEGRAL catalog. The point source located in MGRO J2019+37 circle, IGR J20188+3647, is identified as a transient point source.

upper limits of the fluxes are 2.1×10^{-10} cm^{-2}·s^{-1} for 10–31 GeV, 8.0×10^{-11} cm^{-2}·s^{-1} for 31.1–97 GeV, and 5.0×10^{-11} cm^{-2}·s^{-1} for 97–300 GeV, respectively.

2.2 INTEGRAL IBIS/ISGRI hard X-ray

IBIS (Imager on Board the INTEGRAL Satellite) is one of the instruments of the INTEGRAL X-ray telescope. It works in the energy range from ∼15 keV to several MeV. The FOV of IBIS is 8.33°×8.00° (19°×19°) for fully (50%) coded mode, and the angular resolution (full width at half maximum, FWHM) is 0.2°. There are two detectors: the Integral Soft γ-Ray Imager (ISGRI), which is a semi-conductor array optimized for lower energies (18 keV–1 MeV), and the PIxelated Ceasium Iodide (CsI) Telescope (PICsIT), which is a crystal scintillator sensitive for higher energies (175 keV–10 MeV) [21].

The data and standard analysis software OSA10.0 are downloaded from the INTEGRAL official website[1]. In this analysis we adopt the ISGRI data recorded from 2002 to 2012 for all observing numbers. Due to the quality of achieved data, we restrict the analysis to the energy range 20–200 keV, and divide the data into two bands, 20–60 keV and 60–200 keV respectively. Fig. 2 shows the count rate maps in these two energy bands. These maps are smoothed with a 0.25° width Gaussian kernel. The circle shows the MGRO J2019+37 region with a diameter of 1°, and the white squares show the positions of the sources discovered by INTEGRAL. IGR J20188+3647,

1) http://www.isdc.unige.ch/integral/archive

which is identified as a supergiant fast X-ray transient (SFXT) source, shows a fast rise (10 minutes) followed by a slow decay (50 minutes) [22], and thus may not be the counterpart of the extended TeV source MGRO J2019+37. According to these count rate maps, there is no significant excess coincident with MGRO J2019+37. We will estimate the upper limits of MGRO J2019+37 in the hard X-ray band.

A circle with radius of 0.54° centered on MGRO J2019+37, which encloses 68% of the events from the MGRO J2019+37 extended area taking into account the point spread function (PSF) of ISGRI, is used to calculate the count rate. The expected background count rate is estimated from six other circular regions with the same radius but 1.28° away from the center of MGRO J2019+37. We use the Helene method [23] to calculate the 95% c.l. upper limit of the count rate. Since there is no spectral analysis script for extended source analysis in OSA10.0 software, we adopt a method proposed by the Swift-BAT collaboration [24] to derive the flux of an extended source through comparing the count rate with that of the standard candle Crab Nebula. The source flux can be calculated by

$$\text{source flux}=\frac{\text{source count rate}}{\text{Crab count rate}}\times\text{Crab flux} \qquad (1)$$

in each energy band. To test this method, we apply it to the point sources Cyg X-1 and Cyg X-3, which are close to MGRO J2019+37 as shown in Fig. 2. We compare the fluxes derived by this method with that derived by the standard method for point source analysis conducted by the OSA10.0. Although the spectral shapes of Cyg X-1 and Cyg X-3 are very different from that of the Crab Nebula, the fluxes obtained by the two methods are consistent with each other within 10%. To estimate the flux upper limit from MGRO J2019+37, a power-law spectrum with an index of 2.0 is assumed in this work, which is very closed to the Crab Nebula spectrum. Therefore, the systematic error is expected to be smaller than 10%. The final 95% c.l. upper limits are 1.4×10^{-4} cm^{-2}·s^{-1} for 20–60 keV and 6.0×10^{-5} cm^{-2}·s^{-1} for 60–200 keV.

2.3 XMM-Newton soft X-ray

XMM-Newton has observed the MGRO J2019+37 extended region with the European Photon Imaging Camera (EPIC). EPIC has one pn and two MOS cameras, which covers the energies from 0.2 to 12 keV with an energy resolution of 0.15 keV at 1 keV. Their FOV is 30', and the on-axis resolution angle is about 6" (FWHM) and 15" (half-power diameter).

There are four archival observations of the MGRO J2019+37 extended region. Two of the observations focus on the pulsar wind nebula (PWN) G75.2+0.1. The third points to IGR J20188+3647 and the fourth points to MGRO J2019+37. The pulsar PSR J2021+3651 and its PWN G75.2+0.1, HII regions sh2-104 and WR141 have been detected by EPIC in this extended region. The mosaic image of this region can be found in Fig. 3, which is presented in Ref. [25]. There are no other candidate sources in the 1° region of MGRO J2019+37. The PWN and HII region might be VHE emitters. Therefore we choose PWN G75.2+0.1 and HII region sh2-104 for spectral analysis.

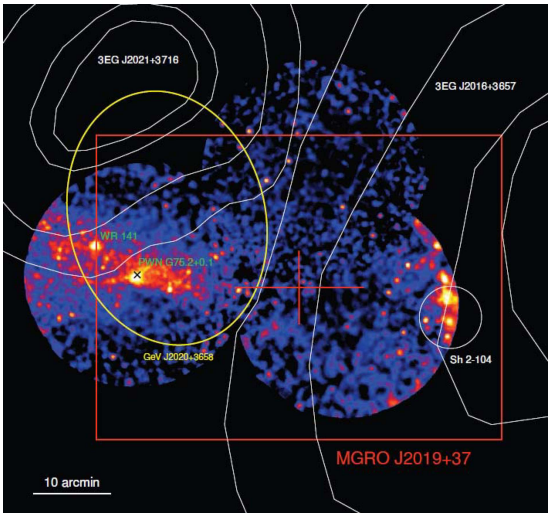

Fig. 3. (color online) XMM-Newton background subtracted and exposure corrected X-ray (1–8 keV) mosaic image of the MGRO J2019+37 region, which is presented in Ref. [25]. The central cross and box indicate the centre of gravity and its positional uncertainty including statistic and systematic errors of the TeV emission from MGRO J2019+37 [6]. The black cross indicates the position of PWN G75.2+0.1. This picture also includes the HII region sh2-104 and the Wolf Rayet star WR141. North is up and East is left.

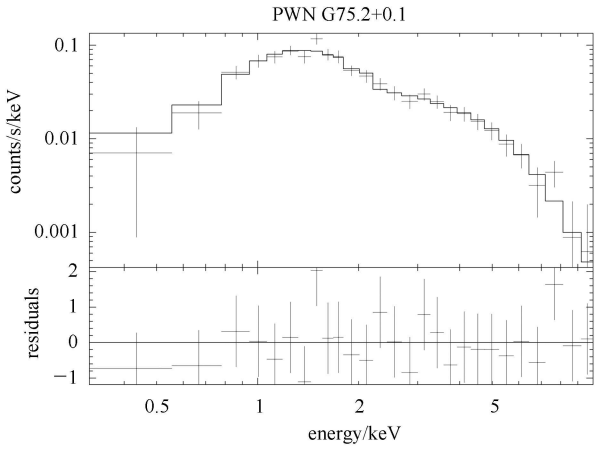

Fig. 4. XMM-Newton MOS2 spectrum for PWN G75.2+0.1 (top panel) and the fit residuals (bottom panel) using an absorbed power-law model.

Table 1. The spectral fitting results obtained using XMM-Newton data.

source name	model	$n_{\rm H}/(10^{22}$ cm$^{-2})$	Index	Flux/(2–10 keV, erg·cm^{-2}·s^{-1})
PWN G75.2+0.1	absorbed power-law	0.31	$1.44^{+0.18}_{-0.17}$	2.62×10^{-12}
sh2-104	absorbed power-law	2.70	$2.09^{+0.88}_{-0.73}$	4.54×10^{-13}

The data from both the MOS and pn instruments were analyzed using the XMM Science Analysis Software (SAS[1)]) version 13.0.1 with the most recent calibration files. The event files were created from observation data files (ODFs) using the SAS tasks epchain and emchain. The events were then filtered to retain only patterns 0 to 4 for the pn data (0.2–15 keV) and patterns 0 to 12 for the MOS data (0.2–12 keV). The data were further filtered to remove the time intervals of high background rates. The observational IDs of the data we finally used for spectral analysis are 0404540101 (MOS2 for G75.2+0.1) and 0510011401 (pn for sh2-104). Ancillary response files and redistribution matrix files are calculated for the corresponding detector regions. We then extract the MOS and pn spectra of the interested source regions.

For PWN G75.2+0.1, we select the extended region with an ellipse (major radius 6.0' and minor radius 3.7'), to subtract the central pulsar. The background is extracted from the off-source region near the source. We employ the X-ray spectral fitting package XSPEC version 12.7.1[2)] to extract the source spectrum. An absorbed power-law model is used to fit the data. The best-fit result and residual of the MOS2 observation of PWN G75.2+0.1 are shown in Fig. 4. For sh2-104, a 0.7' circular area is selected as the source region. Procedure similar to that for PWN G75.2+0.1 analysis is adopted to extract the spectrum. The results are shown in Fig. 5. The fitting results are listed in Table 1.

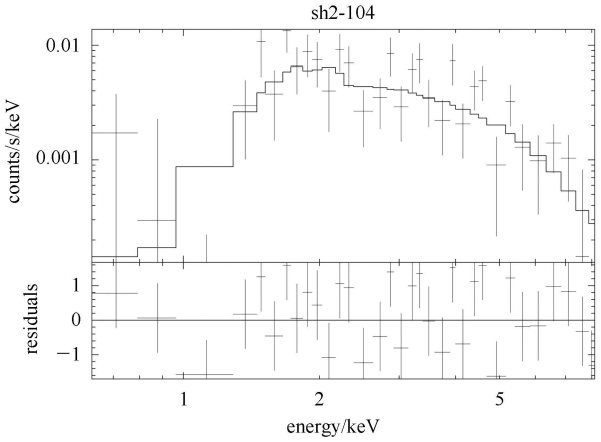

Fig. 5. XMM-Newton pn spectrum for HII region sh2-104 (top panel) and the fit residuals (bottom panel) using an absorbed power-law model.

3 Discussion

The multi-wavelength observational results of MGRO J2019+37 are shown in Fig. 6. Here the XMM-Newton results are the de-absorbed power-law spectrum from PWN G75.2+0.1. Based on the Milagro and ARGO-YBJ data, we find the VHE γ-ray spectrum peak at $\sim$10 TeV, which is higher than most of the known TeV emitters[3)].

Up to now (February 2014), only one of the 147 TeV sources shows similar peak energy to MGRO J2019+37, the peak energy of the PWN Vela X being around 13 TeV [26].

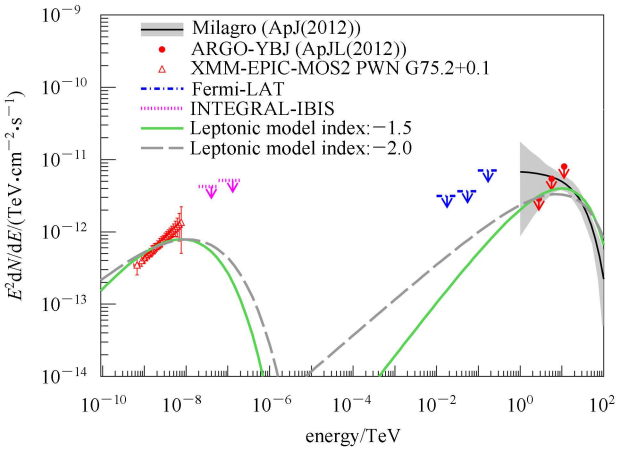

Fig. 6. (color online) Multi-wavelength spectrum of MGRO J2019+37. The shaded region indicates the best-fit spectrum and the 1σ uncertainty region as measured by Milagro [15]. The solid circles with arrows above 1 TeV show the upper limits derived by ARGO-YBJ [5]. The dots with arrows at keV and the dotted line with arrows at GeV show the upper limits derived using data observed by INTEGRAL-IBIS and Fermi-LAT, respectively. The triangles show the flux of PWN G75.2+0.1 using XMM-Newton data. The solid line and break line show the two leptonic model expectations as described in the text.

VERITAS has resolved the emission of MGRO J2019+37 into a complex γ-ray emission region, which is likely composed of multiple sources. If these sources are independent of each other, we would expect the probability of having such a special spectrum with peak energy

1) http://xmm.esa.int/sas/
2) http://heasarc.nasa.gov/xanadu/xspec/
3) http://tevcat.uchicago.edu/

around 10 TeV to be very low. Therefore, it is natural to expect that these complex γ-ray emissions might have the same origin. MGRO J2019+37 is bright and extended in TeV band, without counterpart in other wavelengths. All these properties make it a mysterious "dark" accelerator which radiates VHE γ-rays. Understanding its VHE γ-ray emission mechanism will be interesting and important.

It is worth noting that the observation periods do not fully overlap for these detectors. Assuming a distance of 1–2 kpc for this source, the angular extension $\sigma=0.32^\circ$ will correspond to a length scale of 5–10 pc, which implies a shortest variation time scale of 15–30 years. Therefore, we do not expect a significant flux variation over the whole extended region during the observation time, 2002–2012, of this work.

PWNs are a prominent class of VHE γ-ray sources. G75.2+0.1, PWN of the pulsar PSR J2021+3651, is a possible candidate to power MGRO J2019+37. The spin down power is $\dot{E}=3.4\times10^{36}$ erg s^{-1}. The γ-ray flux integrated from 1 to 100 TeV based on the Milagro spectrum is $F_\gamma=3.2\times10^{-11}$ erg·cm^{-2}·s^{-1}. The estimated distance of PSR J2021+3651 ranges from 2 to 12 kpc [27, 28]. The γ-ray luminosity of this source is:

$$L_\gamma=F_\gamma\times(4\pi d^2)=1.5\times10^{34}(d/2\mathrm{kpc})^2\mathrm{erg\cdot s^{-1}}. \quad (2)$$

The efficiency of VHE γ-ray emission to the spin down power is $L_\gamma/\dot{E}=0.44\%(d/2\mathrm{kpc})^2$. This is consistent with the range of the γ-ray efficiency $\eta_\gamma=10^{-4}$–0.1 found for other PWNs [29].

In the PWN scenario, we could expect a leptonic origin for the multi-wavelength emission of MGRO J2019+37. The γ-ray morphology of a PWN might not be necessarily the same as the X-ray morphology, and the γ-ray luminosity can be also much higher than the X-ray luminosity [30]. If a supernova explosion occurs in an inhomogeneous medium, the resulting asymmetric reverse shock will push the pulsar to the direction away from the higher density medium. In such a scenario, the particles responsible for the γ-rays could be the "relics" of the PWN, while those responsible for X-rays could be newly accelerated ones. Therefore, the X-ray image shows displacement compared with the γ-ray image. The particle spectrum needed to produce X-ray may be also different from that required to produce γ-rays.

It is also possible that the γ-ray emission is produced by hadronic cosmic ray interactions, and the X-ray emission is produced by high energy electrons. In this scenario, there should be more degrees of freedom of the modeling because there is no direct connection with the multi-wavelength data. In the following, we will discuss both the leptonic and hadronic models and explain the multi-wavelength data of MGRO J2019+37.

3.1 Leptonic model

A simple leptonic model is constructed to interpret both the X-ray emissions from PWN G75.2+0.1 and γ-ray emissions from MGRO J2019+37. We assume a uniform distribution of electrons in the vicinity of MGRO J2019+37. VHE γ-ray emission is produced by the inverse Compton scattering of electrons with the interstellar radiation field (ISRF[1)],) including the cosmic microwave background, infrared and starlight [31]. The X-ray emission is produced by the synchrotron radiation of the electrons, within a confined region surrounding the PWN where the magnetic field strength is expected to be higher than the average value in the interstellar medium. A filling factor f is introduced to describe the fraction of the X-ray emitting volume to the γ-ray emitting volume.

The electron spectrum is assumed to be a power-law function with an exponential cutoff $\mathrm{d}N/\mathrm{d}E \propto E^{-\alpha}\exp(-E/E_\mathrm{c})$, where N is the number of electrons, E is the electron energy, α is spectral index and E_c is cutoff energy. Since most of the observations give upper limits, we cannot put good constraints on the model parameters. We choose two values of the electron spectral indices, $\alpha=1.5$ and 2.0, for illustration. It is possible for a PWN to give an electron spectrum harder than 2, e.g., the Crab nebula [32]. For $\alpha=1.5$, we have $E_\mathrm{c}\approx50$ TeV, the total energy of electrons above 1 GeV $W_\mathrm{e}(>1\ \mathrm{GeV})\approx3.2\times10^{46}(d/2\mathrm{kpc})^2$ erg, the magnetic field to produce X-ray emission of G75.2+0.1 $B\approx30$ μG, and the filling factor $f\approx0.3\%$. For $\alpha=2.0$, we have $E_\mathrm{c}\approx90$ TeV, $W_\mathrm{e}(>1\ \mathrm{GeV})\approx8.4\times10^{46}(d/2\mathrm{kpc})^2$ erg, $B\approx30$ μG, and $f\approx0.24\%$. The model expectations are shown in Fig. 6.

The model gives a marginal fit to the data. However, even for $\alpha=1.5$, the synchrotron spectrum seems softer than the XMM-Newton data of PWN G75.2+0.1. As shown in Table 1, the X-ray spectral index is about 1.44, which corresponds to an electron spectral index $\alpha\approx1.9$. The softening of the expected synchrotron spectrum should be due mainly to the cutoff energy E_c. It is possible that, if PWN G75.2+0.1 is the acceleration source of the high energy electrons, the electron spectrum will be harder and cutoff at higher energies when close to the acceleration source. The electrons will then diffuse to the entire region of MGRO J2019+37, become softer and cutoff earlier. The cooling time scale for electrons in the ISRF can be estimated as $\tau_\mathrm{cool}\approx3\times10^5(U_\mathrm{ISRF}/\mathrm{eV\,cm^{-3}})^{-1}(E/\mathrm{TeV})^{-1}$ yr, where U_ISRF is the energy density of the ISRF, and E is the energy of the electrons. Given that the lifetime of PSR J2021+3651 is about 17000 yr, the cooling energy of electrons can be as high as tens of TeV, which is consistent with the required value to fit the data. We can also estimate the diffusion

1) We adopt the local results of the ISRF as an approximation.

scale of the electrons. Assuming a diffusion coefficient of 10^{30} cm^2·s^{-1} (approximate value for TeV particles in the Galactic disk [33]), the diffusion length is estimated to be $\sim 300(D/10^{30}\,\mathrm{cm^2\cdot s^{-1}})^{0.5}(t/17000\mathrm{yr})^{0.5}$ pc. Such a value seems too large compared with the spatial extension of MGRO J2019+37. It seems that the VHE γ-ray emission should come from newly accelerated electrons if this scenario works. Detailed modeling will depend on the time-dependent injection and diffusion of the electrons, which is beyond the scope of this work. In this scenario we could expect an energy-dependent γ-ray morphology to be the same as that for HESS J1825−137 [34]. Future γ-ray facilities with higher sensitivity and angular resolution may test this scenario [35].

The current spin down power of PSR J2021+3651 is $\dot{E}$=3.4×10^{36} erg·s^{-1}. For an estimated age of about 17000 years, the time integrated spin down energy is higher than 1.8×10^{48} erg. Thus the energy fraction transferred to high energy electrons is then $\eta_e \approx (2 \text{ to } 5)\%(d/2\mathrm{kpc})^2$. It shows that PSR J2021+3651 should be enough to power the γ-ray emission of MGRO J2019+37.

An alternative scenario is that the electrons are accelerated in a diffuse region, by e.g. the ensemble of massive OB association in the Cygnus region [36]. In this scenario the non-coincidence of the X-ray image and γ-ray image can be easily understood. The existence of acceleration in the extended region of MGRO J2019+37 may also explain the required hard electron spectrum to reproduce the Milagro measurement and ARGO-YBJ upper limits. However, the fit to the XMM-Newton spectrum is not good enough in this scenario. Furthermore, special treatment of the particle diffusion will be also needed to avoid too large an extension of the source region.

3.2 Hadronic model

γ-ray emission can be also produced through the decay of neutral pions, which are produced in inelastic collisions between accelerated cosmic ray nuclei and the ambient interstellar medium. We still assume an exponential cutoff power law for the spectrum of the accelerated nuclei (protons for simplicity). The expected γ-ray spectra for two illustration values of proton spectral indices, α_p=1.5 and 2.0, are shown in Fig. 7. For α=1.5 (2.0), the adopted cutoff energy is 200 (500) TeV, and the total energy of protons above 1 GeV is 6.4(16)×10^{49} $(d/2\mathrm{kpc})^2(n/\mathrm{cm^{-3}})^{-1}$ erg.

Figure 7 shows that the hadronic model can barely fit the γ-ray data. The exponential cutoff power-law spectrum of protons seems to be too broad compared with the peak behavior of the VHE γ-ray spectrum, unless the proton spectral index is much harder. The required total energy of protons seems to be higher than the above estimated energy released from spin down of PSR J2021+3651. It is possible that the total energy release of PSR J2021+3651 is higher than 1.8×10^{48} erg because the rotation of the pulsar should be faster in the past. Another possibility is that these protons were accelerated by the remnant of the supernova which produced PSR J2021+3651. The total energy of protons seems to be consistent with the canonical value of ∼10% of the total kinetic energy released from a typical supernova explosion, say 10^{51} erg. However, the constraints from particle diffusion as discussed in Section 3.1 is also applied here. A high density concentration or a low diffusion coefficient around MGRO J2019+37 may be helpful to avoid the too large extension problem due to diffusion. Similar to the leptonic scenario, the protons can be also accelerated diffusively in the extended region of MGRO J2019+37.

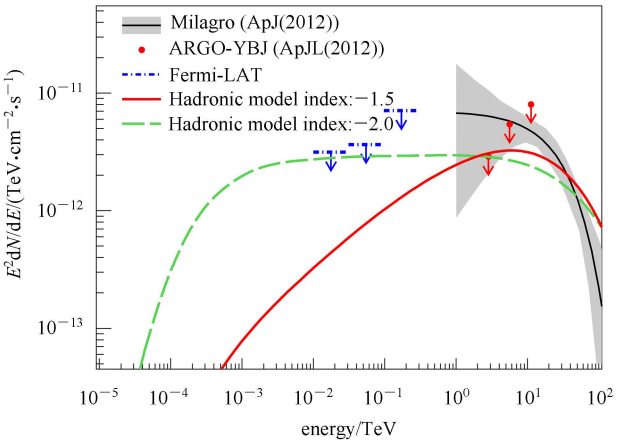

Fig. 7. (color online) Two hadronic model expectations of the γ-ray spectrum of MGRO J2019+37, compared with the data.

4 Summary

MGRO J2019+37 is a special TeV γ-ray source in the northern sky. This paper presents a collection of the multi-wavelength observations of MGRO J2019+37 from X-ray to TeV γ-ray bands. The available archival data in the direction of MGRO J2019+37 from XMM-Newton at soft X-ray band, INTEGRAL at hard X-ray band and Fermi-LAT at GeV γ-ray band are analyzed. There is no corresponding extended signal in INTEGRAL and Fermi-LAT data, and the flux upper limits are obtained. In XMM-Newton data, emissions from the PWN G75.2+0.1 and the HII region sh2-104 are found. Spectral analyses of G75.2+0.1 and sh2-104 are performed. The possible multi-wavelength radiation mechanism of the source is discussed. It is shown that a leptonic scenario can marginally reproduce the X-ray to TeV γ-ray data. The PWN G75.2+0.1 of PSR J2021+3651 might be the acceleration source of the high energy electrons. Although the hadronic scenario gives a

worse fit to the data, it should not be excluded, as there is still a lack of high quality data. The diffuse particle acceleration from the ensemble of OB associations, for example, can also explain the observational results.

Due to the lack of detailed observations, no favored model can be obtained right now. To further unveil the puzzle of the dark accelerator MGRO J2019+37, observations with more sensitive instruments at various bands are needed. In the near future, new EAS experiments such as HAWC, Tibet+MD and LHAASO are expected to be able to achieve a more accurate observation of γ-ray sources from 40 GeV to 1 PeV. The γ-ray emission mechanism of this source is expected to be uncovered in the new era of VHE γ-ray astronomy.

We are grateful to Long Ji, Jian Li and Yupeng Chen for their help in estimating the hard X-ray spectrum using the INTEGRAL data. We also acknowledge Prof. Carlos Gabriel, Prof. Randall Smith and Ping Zhou for their essential help in the XMM-Newton data analysis.

References

1 Abdo A A et al. arXiv: 1108.1435 [astro-ph.HE]
2 Abdo A A et al. The Astrophysical Journal, 2008, **688**: 1078–1083
3 MA Ling-Ling. A Measurement of the Diffuse TeV Gamma Ray Emission from the Galactic Plane with ARGO-YBJ Experiment. Proceeding of the 32nd International Consmic Ray Conference, Beijing, 2011, **7**: 2–5
4 BI Xiao-Jun et al. The Astrophysical Journal, 2009, **695**(2): 883
5 Bartoli B et al. The Astrophysical Journal Letters, 2012, **745**: L22 (5pp)
6 Abdo A A et al. The Astrophysical Journal, 2007, **658**: L33–L36
7 Abdo A A et al. The Astrophysical Journal, 2007, **664**: L91–L94
8 Abdo A A et al. The Astrophysical Journal, 2009, **700**: L127–L131
9 Amenomori M et al. Study on the Energy Spectrum of Cygnus Region. Proceedings of the 30th International Cosmic Ray Conference. Merida, Mexico, 2007, **2**: 695–698
10 WANG Yue et al. Chinese Physics C (HEP & NP), 2008, **32**(11): 868
11 Amenomori M et al. The Astrophysical Journal, 2010, **709**: L6
12 Bartoli B et al. The Astrophysical Journal, 2013, **779**: 27
13 Bartoli B et al. The Astrophysical Journal, 2012, **760**: 110 (6pp)
14 Bartoli B et al. The Astrophysical Journal, 2013, **767**: 99 (6pp)
15 Abdo A A et al. arXiv: 1202.0846v1 [astro-ph.GA]
16 Weinstein A et al. arXiv: 0912.4492 [astro-ph.HE]
17 Aliu E. arXiv: 1110.4656v2 [astro-ph.HE]
18 Paredes J M et al. Astronomy and Astrophysics, 2009, **507**(1): 241–250
19 Abdo A A et al. The Astrophysical Journal, 2011, **734**: 28 (9pp)
20 Abdo A A et al. The Astrophysical Journal, 2009, **700**: 1059–1066
21 IBIS Analysis User Manual. http://www.isdc.unige.ch/integral/download/osa/doc/10.0/osa_um_ibis/index.html
22 Sguera V. arXiv: 0902.0245v1 [astro-ph.HE]
23 Helene O. Nucl. Instrum. Methods, 1983, **212**: 319
24 Tueller J et al. The Astrophysical Journal Supplement Series, 2010, **186**: 378
25 Zabalza V et al. High Energy Phenomena in Massive Stars ASP Conference Series, 2010, **422**: 186
26 Aharonian F et al. Astronomy and Astrophysics, 2006, **448**(2): L43–L47
27 Abdo A A et al. The Astrophysical Journal, 2009, **700**: 1059–1066
28 Hessels J W T et al. The Astrophysical Journal, 2004, **612**: 389–397
29 Hessels J W T et al. The Astrophysical Journal, 2008, **682**: L41
30 Mattana F et al. The Astrophysical Journal, 2009, **694**: 12
31 Porter T A, Strong A W. Proceedings of the 29th International Cosmic Ray Conference. Pune, India, 2005, **4**: 77–80
32 YUAN Qiang et al. The Astrophysical Journal, 2011, **730**: L15 (5pp)
33 Aharonian F et al. Nature, 2006, **439**: 695
34 Aharonian F et al. Astronomy and Astrophysics, 2006, **460**(2): 365–374
35 CHEN Song-Zhan. SCIENCE CHINA Physics, Mechanics & Astronomy, 2013, **56**: 1454
36 Bykov A, Toptygin I. Astronomy Letters, 2001, **27**: 625